Characterization of Frequency and Flow Response of Magnetically Actuated Swimming Millirobots with Asymmetric Helical Body

Marcus C. J. de Boer

Abstract— Currently, one of the treatment methods for patients with acute proximal deep vein thrombosis is catheter-directed thrombolysis or mechanical thrombectomy. One of the factors that influence the complication rate of these treatments is the reachability of the thrombus. To overcome this increased complication risk, untethered magnetic swimming robots could be an addition to the mechanical treatment approach.

In this paper, the swimming behaviour of such a robot with an asymmetrical helical body and varying magnetic volume was characterized by assessing frequency and flow response *in-vitro* in water. Here it became apparent that the robots had different swimming speeds for each orientation. Furthermore, linear relations between actuation frequency and flow and translational speed were found for flow responses for all measurements and for frequency responses until the frequency where the robot could no longer overcome frictional forces (step-out frequency). Moreover, different magnet volumes showed different frequency responses with no direct relation between them. This gave more insight into other influencing factors such as magnetic force and frictional force. Additionally, using experimental data and previous research, step-out frequencies and maximum flow rates were estimated for the robots in blood. Besides, testing showed that the rotating permanent magnet which is used to actuate the robot is limited at 42 Hz. This was identified to be the limiting factor in achieving higher translational speeds. The last finding was that, when changing the swimming direction, the robot seemed to flip randomly, especially when further away from the rotating permanent magnet.

For future research, it is essential to test the asymmetrical design in blood as well. By doing this, the accuracy of the estimations of the robot's performance in blood can be assessed. This could allow direct translation of test results in water setups to outcomes in blood. To overcome higher flow rates, which would be necessary for possible future clinical applications, the maximum frequency of the actuator should be increased. Furthermore, to counter the flipping of the robot, a different control method where the actuator is no longer stationary and/or a change in design towards a symmetrical body is recommended.

I. INTRODUCTION

Venous thromboembolism (VTE) occurs when a thrombus forms in a vein. VTE encompasses deep vein thrombosis (DVT) and pulmonary embolus (PE). This disorder knows approximately half a million symptomatic events per year in the European Union alone. Currently, treatment of VTE initiates with 5 to 7 days of administering thrombolytics [1]. The first three months after this treatment recurrence, extension of the thrombus and embolization of the thrombus are closely monitored. After the three-month time point, anticoagulation is used to prevent late recurrence. In selected patients with acute proximal DVT, catheter-directed thrombolysis or mechanical thrombectomy may be used to reduce acute symptoms [2]. However, these treatments could cause a variety of complications. For any patient, the complication rate is dependent on the demographics of the patient, vascular anatomy, co-morbid conditions, clinical presentation, the procedure being performed, and the experience of the operator. [3]. Moreover, the chemical (part of the) treatment can lead to adverse effects such as bleeding, hypotension, allergic reactions, angioedema, anaphylactic shock, and reperfusion arrhythmias [4].

Untethered magnetic robots (UMRs) could be an addition to the mechanical treatment methods. UMRs are magnetized helical-shaped milli-devices driven by a rotating external magnetic field. These robots have been extensively studied in the fields of cargo transportation, cell manipulation, toxic substance removal and micromanipulation [5]. In the case of VTE treatment, the latter could be considered.

Leclerc *et al.* have already disrupted a 1-hour-old thrombus using such a UMR [6] [7]. Removal of a bigger, partially dried thrombus, proved to be more challenging due to the lack of torque of the UMR. To overcome this, Lu *et al.* introduced 18 designs with a larger volume of permanent magnets and variations of head drill shape and body helix designs [8]. Two of the designs were further analysed based on their swimming and path-tracking performance. The combination of the asymmetric helical body and the screw-shaped body with helical tip (see Figure 3) proved to be most suited for thrombus removal, where the asymmetric helical body is most suited for reducing the size of the thrombus and the screw-shaped body with helical tip is suited for the disruption and retrieval of small pieces of the thrombus. In their research, the UMRs are actuated using non-moving electromagnets (EMs) [6]. Two EMs oriënted along different axes provide a rotating magnetic field when a sinusoidal current with a phase shift is applied. Additional EMs enable directional use. The advantage of this system is that high actuation frequencies can be achieved and no expensive electric motors or heavy rotating parts within the operating room are required. However, this system cannot be used *in-vivo*, since the field-of-view of clinical imaging systems, which is necessary for deep-tissue tracking, would be limited by the placement of the EMs.

Therefore, Ligtenberg *et al.* [9] moved towards a scalable X-ray-guided robotic platform, which uses a rotating permanent magnet (RPM) as the actuator. Recently, this platform was used to translate the UMRs into *ex-vivo* trials where directional control inside a porcine aorta model was achieved [10]. Besides, hemobiocompatability, wireless locomotion in arterial flow and directional control and steering were researched.
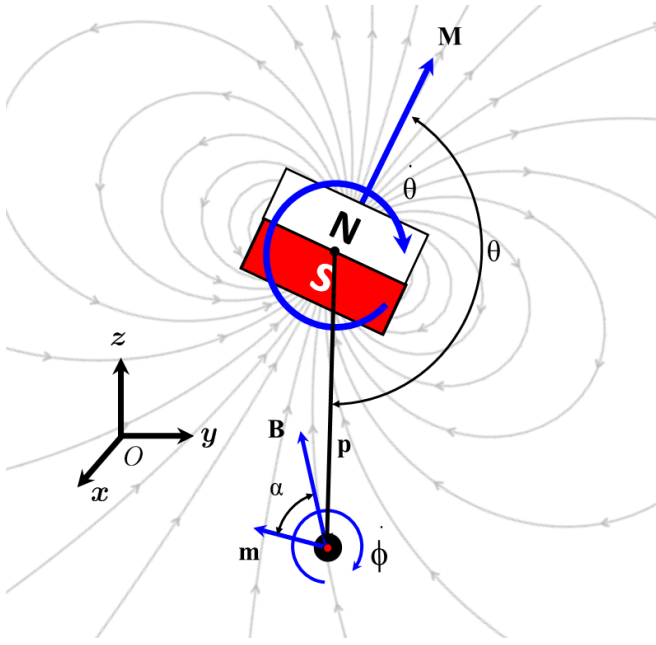
Fig. 1: The schematic shows the world frame of the magnetic dynamics, where the translational movement direction of the UMR is along the x-axis. Here, vector $\mathbf{p}$ is the vector between the centre of the magnet of the RPM and the centre of the magnet of the UMR, θ is the angle between the magnetic moment of the RPM $\mathbf{M}$ and vector $\mathbf{p}$, α is the angle between the magnetic moment of the UMR $\mathbf{m}$ and the local magnetic field $\mathbf{B}$ and $\dot{\phi}$ is the rotational velocity of the UMR.

The goal of this study is to assess the swimming performance of the asymmetric helical body with a varying amount of magnets in the X-ray-guided robotic platform and to assess the feasibility of this design for feature research. From the two designs proposed by Lu *et al.*, the asymmetric helical body is chosen because the next phase in the *ex-vivo* trails focuses on decreasing the size of the thrombus by drilling. The goal will be achieved by mathematically predicting the translational speed of the device, and analysing experimentally determined translational speeds at varying actuation frequencies and flow rates in an experimental test setup.

II. THEORY

A. Dynamics

To create an understanding of how the UMRs function, the dynamics are analysed. The dynamics of a magnetic device driven by a rotating dipole field have been described by Mahoney *et al.* [11] and Fountain *et al.* [12]. Mahoney *et al.* have used a stationary world frame with axes x,y,z (see Figure1) to describe these dynamics. A magnetic field, generated by the RPM with dipole moment $\mathbf{M}$ generates a local magnetic field vector $\mathbf{B}$ at the position of the UMR, where the magnitude of $\mathbf{M}$ can accurately be approximated

using the point-dipole model:

$$|\mathbf{M}| = \frac{B_r V}{\mu_0}, \qquad (1)$$

where B_r is the residual flux density, which the magnet manufacturer provides, V is the volume of the magnet and μ_0 is the permeability of free space. The position of the UMR relative to the centre of the RPM is the vector $\mathbf{p}$. Using all of the above, the local $\mathbf{B}$ can be computed as follows:

$$\mathbf{B} = \frac{\mu_0}{4\pi|\mathbf{p}|^3}\left[3\frac{\mathbf{p}\mathbf{p}^T}{|\mathbf{p}|^2} - \mathbb{I}\right]\mathbf{M} = \frac{\mu_0|\mathbf{M}|}{4\pi|\mathbf{p}|^3}\begin{bmatrix} 0 \\ \sin(\theta) \\ -2\cos(\theta) \end{bmatrix}, \quad (2)$$

where $\mathbb{I}$ is the identity matrix and θ describes the angle between the dipole moment of the RPM and the z-axis. The magnetic torque produced on the UMR is calculated using $\tau = \mathbf{m} \times \mathbf{B}$, where the dipole moment of the UMR $\mathbf{m}$ is calculated using Formula 1. Using this magnetic torque and a linear drag torque coefficient c, the UMR's rotational dynamics are:

$$-c\dot{\phi} + |\mathbf{m}||\mathbf{B}|\sin(\alpha) = 0, \qquad (3)$$

where, $\dot{\phi}$ is the rotational speed of the UMR. The speed at which the drag torque equals the magnetic torque is called the step-out speed or step-out frequency. Since $\dot{\phi}$ is linearly coupled to the rotating actuator below this step-out frequency, according to Formula 2, the actuator must be driven so that the rotational velocity $\dot{\theta}$ is:

$$\dot{\theta} = \frac{\mu_0|\mathbf{m}||\mathbf{M}|}{8\pi|\mathbf{p}|^3 c}(1 + 3\cos^2(\theta))^{\frac{3}{2}} = K(1 + 3\cos^2(\theta))^{\frac{3}{2}}. \quad (4)$$

This rotational velocity of the RPM keeps α at $90°$ as $t \to \infty$, which generates the highest possible magnetic torque. In practice, θ is known, $\mathbf{p}$ can be visually measured and an estimate of K ($\hat{K}$) is used as speed coëfficient. If $\hat{K} \leq K$, α converges to $sin^{-1}(\hat{K}/K)$. If $\hat{K} > K$, no steady-state exists, which will cause the UMR and RPM to step out of synchronization. K can be determined by increasing $\hat{K}$ until the device steps out of synchronisation, at which $\hat{K} \approx K$.

When the actuation takes place according to Formula 4, and the device is positioned as in Figure 1, magnetic force can be computed using Formula 2 and $\mathbf{F} = (\mathbf{m} \cdot \nabla)\mathbf{B}$:

$$\mathbf{F} = \frac{3\mu_0|m||\mathbf{M}|}{4\pi|\mathbf{p}|^4}\left(\frac{1 + \cos^2(\theta)}{\sqrt{1 + 3\cos^2(\theta)}}\right)\begin{bmatrix} 0 \\ -1 \\ 0 \end{bmatrix}. \qquad (5)$$

The direction of this force is $\mathbf{\Omega} \times \mathbf{p}$, where $\mathbf{\Omega}$ is the angular velocity vector of the RPM. The magnitude $|\mathbf{F}|$ of Formula 5 varies from 94,3% to 100% of $\frac{3\mu_0|\mathbf{m}||\mathbf{M}|}{4\pi|\mathbf{p}|^4}$ as θ changes which makes the magnetic force relatively constant. When the magnet is not actuated satisfying Formula 4, the direction of this magnetic force no longer satisfies $\mathbf{\Omega} \times \mathbf{p}$ and the UMR will be attracted by the magnet [11].

Besides rotational dynamics, the dynamics of the device in a fluid are important to estimate translational velocities. Li *et al.* describes that the translational resistive force balance (along the x-axis in Figure 1) is made up of a drag force F_d

and a viscous force F_μ [13]. F_d can be computed using the drag equation:

$$F_d = \frac{1}{2}\rho u^2 c_d A, \qquad (6)$$

where ρ is the mass density of the fluid, u is the flow velocity relative to the object, A is the reference area and c_d is the drag coefficient, which takes geometry, skin friction and form drag into account. The drag coefficient is difficult to analytically derive for complex shapes like that of the UMR. However, Stokes' law states that for a small spherical particle in a viscous fluid with laminar flow, drag force can be computed according to:

$$F_d = 6\pi\mu R v, \qquad (7)$$

where μ is the dynamic viscosity of the fluid, R is the radius of the spherical object and v is the flow relative to the object. By assuming the UMR is a spherical particle in laminar flow a basic understanding of influencing factors on the drag of the UMR can be formed. Laminar flow occurs at Reynolds numbers Re below $Re \approx 2040$ [14]. Reynolds number is defined as:

$$R_e = \frac{\rho v D}{\mu}, \qquad (8)$$

where ρ is the density of the fluid, v is the speed of the UMR relative to the fluid, D is the length of the UMR and μ is the dynamic viscosity of the fluid. For a more accurate representation of the solution for the drag force of the UMR, computer simulation or experimental derivation is necessary. This however falls not within the scope of this research.

Furthermore, there is a viscous force F_μ which drives the UMR forward. This force is calculated using tangential force and normal force coefficients, which are only related to the geometry of the UMR. Since the UMR that is studied has a complex shape which has not been defined mathematically, these coefficients are estimated and from this, resulting translational velocity and torques are computed using Stokeslet analysis, which will be further discussed in the Methods section. (see III-B). Vertical forces on the device are constant if the swimming direction of the UMR is solely along the x-axis and Formula 4 is satisfied. In this case, only gravitational and buoyancy forces are acting on the UMR. These forces are computed by $F_z = mg$ and $F_b = V\rho g$ respectively, where, m is the mass of the UMR, g gravitational force in the fluid, V is the volume of the UMR and ρ is the density of the fluid. If the net force of the gravitational and buoyancy force does not equal 0, there will eventually be interaction with the lumen which causes a normal force F_n to act on the UMR as well. This normal force will in turn result in a translational frictional force defined by $F_f = \mu_f F_n$, where μ_f is the friction coefficient of the interaction between the UMR and the lumen. All of the influencing forces that are acting on the UMR are summarized in Figure 2. Here, the situation where Formula 4 is not satisfied is used, which will cause a magnetic force F_m between the UMR and RPM to act in the x,z-plane. This will result in the following force balance, where F_f and F_N only exist if there is interaction
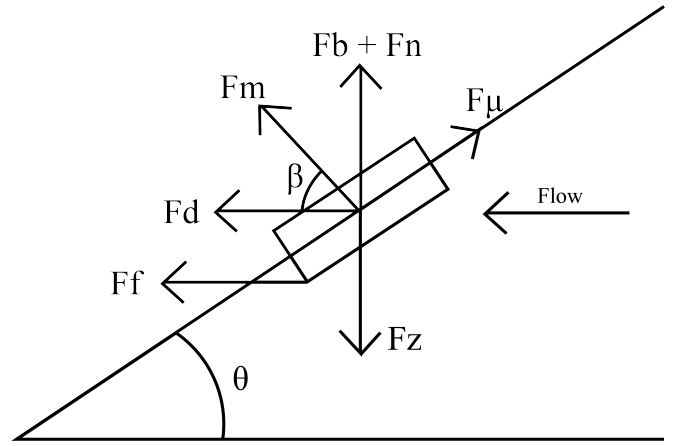

Fig. 2: The Figure illustrates the free-body-diagram of the UMR, where F_d is the drag force, F_m is magnetic force, F_b is buoyancy force, F_n is normal force, F_μ is viscous force, F_z is gravitational force, F_f is frictional force, θ the angle between flow direction and direction of the viscous force and β is the angle between the direction of the magnetic force and the flow direction.
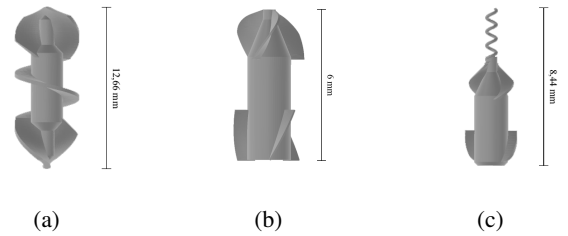

Fig. 3: The three UMR designs that are discussed. (a) The symmetrical design by Khalil *et al.* [10] was made for X-ray-guided control (b) the asymmetric helical body by Lu *et al.* [8] was made for thrombus size reduction (c) the screw-shaped body with helical tip by Lu *et al.* [8] was made for disruption and retrieval of small pieces of the thrombus.

with the lumen:

$$\begin{aligned} F_x &= F_\mu \cos\theta - F_d - F_m \cos\beta - F_f \\ F_y &= F_\mu \sin\theta + F_b - F_z + F_m \sin\beta + F_n. \end{aligned} \qquad (9)$$

In previous research by Khalil *et al.* [10] the influence of fluid relaxation and diameter of the surrounding vessel on the above forces and therefore swimming speeds have been researched as well. Here, it became apparent that at higher fluid relaxation, swimming speed diminishes and that a decrease in vessel diameter causes a higher cylinder-to-vessel ratio, for which there is an observed speed increase.

B. UMR design

UMRs have different geometries depending on the application [5]. The UMRs discussed in this paper have a spherical/helical shape, which allows easy assembly and is useful in micromanipulation applications due to the screw-shaped head. In Figure 3 the shapes of the discussed UMRs are displayed.
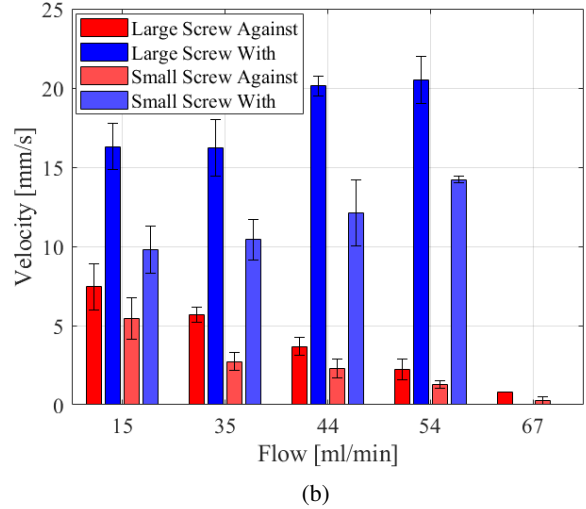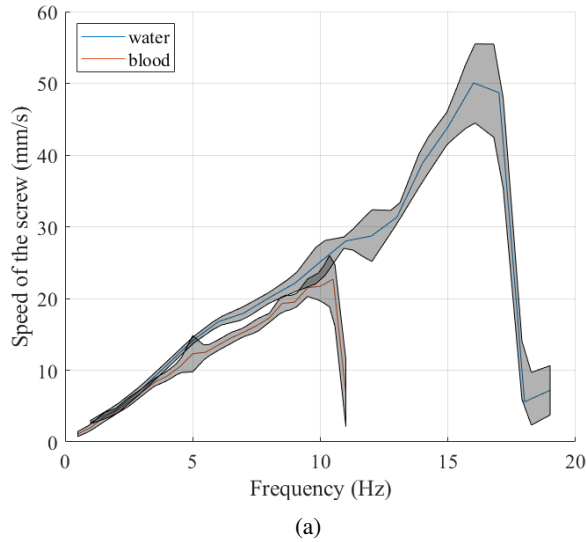
Fig. 4: (a) Frequency response of the full-scale symmetrical helical design in blood and water in the same set-up (tube diameter of 9.525mm). (b) Flow response of the symmetrical helical design in *ex-vivo* set-up. The large screw is the full size of the symmetrical helical design and the small screw is scaled with a factor of 0,75. The UMRs are actuated at 9Hz at a gap of 10 cm with the tube.

The first UMR (Figure 3a) is magnetized using one N45 cylindrical magnet with a diameter and height of 1 mm and has been tested at a variable frequency in water and blood and in variable flow in an ex-vivo setup [10]. The frequency response in blood was assessed for both the full-scale and scaled (factor 0.75) symmetrical helical UMR to assess the influence of its size. The full-scale device showed a step-out frequency of around 26Hz compared to the 9Hz of the scaled version. Because the scaled UMR was more feasible for clinical application due to its size and because translational speeds at an actuation frequency of 9Hz were relatively equal for both UMRs, it was decided to test flow response in blood at an actuation frequency of 9Hz. From this, the influence of using blood instead of water on frequency response and the influence of flow and a different swimming environment of the *ex-vivo* setup on the translational speed of the UMR was derived.

Looking at 0-10 Hz in Figure 4a, and using a linear fit to asses the slope of both measurements, a factor of 1.14 (blood to water slope) is calculated. Furthermore, there's a significantly higher step-out frequency for the water measurement. This can be explained if we assume that the viscosity of the fluid has an impact on the linear drag torque coëfficient c as displayed in Formula 3. Higher viscosity will cause a higher c and therefore a lower step-out frequency. Using Formula 3, if we assume that magnetic torque remains constant, the change factor of c is 1.52 for the step-out frequency of water to blood.

Looking at Figure 4b, a linear relation between flow and translational velocity can be seen for movement with and against flow. Furthermore, it is visible that the larger UMR has higher speeds and that both of the UMRs can withstand a maximum flow of approximately 67 ml/min.

The second UMR (Figure 3b) is the result of experimental research by Lu *et al.* [8]. This research aimed to increase permanent magnet volume to create higher torques used for the micromanipulation of a thrombus and varied the number of helices and the type of drill heads. Here, the design was proven most feasible for thrombus size reduction, which is the reason why this design is further researched in this paper. In the case of this design, up to four 1 mm^3 cube magnets can be inserted. According to Formula 1 and 3, when using the same magnets, the step-out frequency is directly proportional to the number of magnets if the rotational drag coefficient does not change. This is because only magnet volume V is increased.

The third UMR (Figure 3c), a design that resulted from the experimental research by Lu *et al.* [8] as well, managed to retrieve a small remaining piece of a size-reduced thrombus. This design will however not be considered in this paper to keep the focus on thrombus size reduction.

III. METHOD

A. Assembly of the UMRs

The bodies of the UMRs were 3D-printed using a resin 3D printer (Phrozen Sonic Mini 4K Resin 3D, Phrozen Tech Co Ltd, Hsinchu City, Taiwan) using Phrozen Aqua Grey 4K Resin. After enough prints are obtained, the magnets are inserted into the bodies. For this, N45 1 mm^3 cube magnets are used, since these are relatively cheap and fit into the design. In the insertion process, all of the magnet's poles must be directed in the same direction and perpendicular to the rotational axis of the UMR to allow torque by an external rotating magnetic field. The amount of magnets per body is

varied from 1 to 4 and the magnets are fixated using glue. To ensure proper assembly and to verify the feasibility of using X-rays to visualize the UMRs for possible future *ex-* or even *in-vivo* use, X-rays of the UMRs in contrast fluid are made (using Siemens Healthineers Artis Pheno, Erlangen, Germany). Contrast fluids are used since this would also be used in clinical practice to visualise the thrombus size.

B. Stokeslet analysis

The Stokeslet analysis allows the prediction of the translational velocity of the design. This is done by computing the Stokes flow driven by external forces, which in this case is generated by the rotating permanent magnet, at material points on the design in a fluid. For this, an existing MATLAB script by A. Klingner (2023) is used. The script can be found in Appendix A of this paper. This script allows analysis based on the STL file of the UMR. The rotation frequency of the UMR, the radius of the tube, the number of time steps, the scaling of the robot and the viscosity of the surrounding fluid are inputs of the model. The model assumes a perfectly Newtonian fluid, no viscoelastic effects and that there is no direct interaction between the UMR and the tube walls. This model offers substantiation for the results of the frequency response experiment, which is described in the next subsection. To be able to substantiate this experiment, the actuation frequency is varied from 5 Hz to the experimentally determined step-out frequency in steps of 5 Hz. These actuation frequencies are also reversed to see if there is a difference in swimming speeds between orientations of the UMR. The tube radius is set to 4.7625 mm to resemble the setup of the frequency response experiment, time steps to 5 (suggested), scaling to 1 (no scaling) and viscosity of the fluid to the viscosity of water at 20°C, which is 0.0010016 Pa·s [15].

C. Frequency response

The frequency response is measured to identify the translational speeds at different actuation frequencies of different magnet configurations. From this, the step-out frequencies of the UMRs will be determined by identifying the actuation frequency where the translational speed is maximal. Using the relation between frequency response in water and blood (see section II-B), the maximum translational velocity in blood in the same tube can be estimated. Since the new design is asymmetrical, speed variation between orientations will be assessed too.

Firstly, the symmetrical helical design that was used to derive the relation between swimming speeds in water and blood (see section II-B) is tested and compared to this previous research to validate the setup. Then, the test will be repeated for all magnet configurations (1, 2, 3 and 4 magnets) of the new design. This is used to compare the frequency response of these configurations.

The UMR is put in a transparent silicone tube with an inner diameter of 9.525 mm. This tube is filled with water and sealed with two caps. After the tube is secured to a base plate, a robotic manipulator (KUKA KR-10 1100-2,
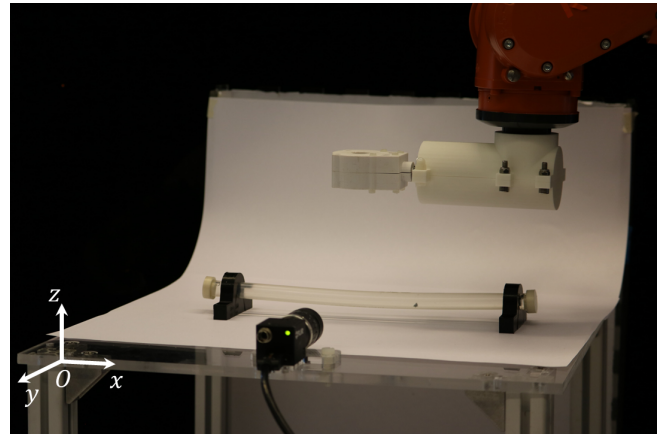

Fig. 5: The experimental setup to asses frequency response consists of two main components: A silicone tube which contains the UMR and the robotic manipulator with RPM attached.

KUKA, Augsburg, Germany) equipped with an RPM, is moved so that the rotational axis of the RPM is parallel to the tube and the RPM is situated above the centre of the tube as seen in Figure 5. The gap between the tube and the RPM is held at 10 cm for the old UMR and at 15 cm for the new UMRs (the asymmetric helical body). The reason for this difference is the strength of the magnets. The magnets of the new UMRs are stronger (cubical instead of cylindrical) and, according to Formula 5, would therefore be more influenced by the magnetic force. Since the goal is to assess the swimming speeds caused by the rotation of the UMR and not because of the movement of the RPM, the RPM remains stationary throughout the experiments. By doing this, the influence of the magnetic force when the robot swims further away from the RPM can also be examined. At least three runs per oriëntation per frequency are required to assess the swimming speeds. Speeds will be measured per 5 Hz up to the frequency where translational speed has declined significantly after the step-out frequency. These measurements are made using a camera (BFS-U3-13Y3C-C USB 3.1 Blackfly® S, FLIR, Wilsonville, United States) that is positioned perpendicular to the length of the tube. From these videos, position over time is obtained using the Tracker (Version 6.1.5, Brown *et al.*, 2023) video analysis software as depicted in Figure 6. The data is processed and illustrated using MATLAB (Version 9.12 (R2022a), The MathWorks Inc., 2022). MATLAB is also used as the control interface of the RPM. This script is found in Appendix B. In the interface, the frequency and the rotational direction of the RPM can be controlled. By switching rotational direction, the swimming direction will change as well. This allows continuous measurements of the forward and backward motion of the UMR during the experiment.

D. Flow response

The flow response is measured to identify translational speeds at different flow rates. If the UMR were to be feasible
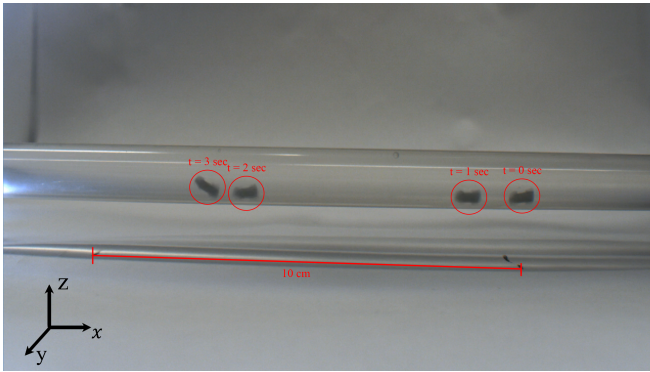
Fig. 6: Here, the position tracking is illustrated. X- and y-coordinates are computed for every frame and scaled using the scaling bar. From this, position over time and speed can be obtained.
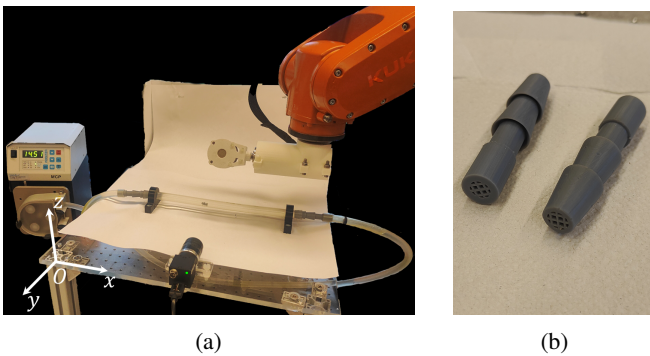

(a)   (b)

Fig. 7: The experimental setup to asses flow response consists of three main components: (a) The water loop which connects the pump with the transparent silicone tube which contains the UMR, the robotic manipulator with RPM attached and, (b) to prevent the UMR from going outside this tube, a pair of 3D printed filters.

for *in-vivo* use, it would have to withstand the high flow rates in the human arteries. Therefore, it is necessary to validate the UMR's behaviour in flow and to assess the maximum flow it can withstand.

The setup of this experiment is similar to the frequency response measurement, however, the tube is now connected to a peristaltic pump (Masterflex® Ismatec® MCP Standard Digital Peristaltic Pump Drive with PRO-380 pump head, Antylia Scientific, Glattburg, Switzerland) with an adjustable flow rate (see Figure 7). The validity of the flow indicator on the pump is examined using a large measuring glass and a timer.

Firstly, the symmetrical helical UMR design is actuated at 9 Hz with a gap of 10 cm. This configuration was used in the previous flow response experiment as depicted in Figure 4b. The 9 Hz actuation frequency was picked since it is slightly below the step-out frequency of the symmetrical helical design in blood. Here, the swimming velocity was assessed from 15 ml/min to 67 ml/min as done for Figure 4b. To determine the relation between the flow response between water and blood at the same actuation frequency, this will be done in the water flow setup as well.

Secondly, the symmetrical helical UMR design is actuated at 14 Hz at a gap of 10 cm. This is slightly below its step-out frequency in water (see II-B). From this, a comparison between flow response in water and blood at (slightly below) step-out frequency can be made.

Lastly, all magnet configurations of the asymmetric helical body are assessed slightly below the step-out frequency which is determined in the frequency response experiment (see III-C). Since this actuation frequency causes the highest translational velocity we can determine the maximum flow the UMR can withstand in this setup. Using the experimentally determined relations between water and blood of the old symmetrical helical design, predictions about the flow response of the asymmetric helical body in similar circumstances as the *ex-vivo* setup can be formed. Furthermore, differences in flow response between magnet configurations are assessed.

Again, measurements are done using the FLIR Blackfly camera and analysed, processed and illustrated using Tracker and MATLAB. Since it is symmetrical, the old design requires three runs against and three runs with flow. For the new design, this is required for each orientation, because of the asymmetrical design.

IV. RESULTS

A. Assembly

During the assembly process, two main problems arose: The success rate of the 3D prints was inadequate and the insertion of four magnets proved to be strenuous. Since there was no printer available which could print the fins at the designed thickness, to overcome the first problem, the fin thickness was increased from 100 μm to 150 μm. This improved the success rates of the prints significantly, which is why it was decided to keep this property for future use. The second problem could not be solved without coming up with a completely new assembly method which was why it was decided to insert up to three magnets and assess those. The reason why the fourth magnet could not be inserted was because the repellent magnetic force between magnets when compressing them into the UMR caused all the magnets to "jump" out of the UMR before fixation could take place. After enough UMRs were provided with the magnets, X-rays were made to identify the magnet position within the devices and verify the feasibility of possible future X-ray tracking. In the X-rays, displayed in Figure 8, the magnets provide a significant contrast with its background. However, the contrast between the background and the body of the UMR is less clear, which could be problematic when determining the orriëntation of the device. The position of the magnets within the UMR is important for the balance of the device. It can be seen that the position of the single magnet is completely against the pointy head, while the position of the two- and three-magnet configuration seems to be equally spaced over the whole cavity of the UMR. This makes sense since the magnets repel each other.
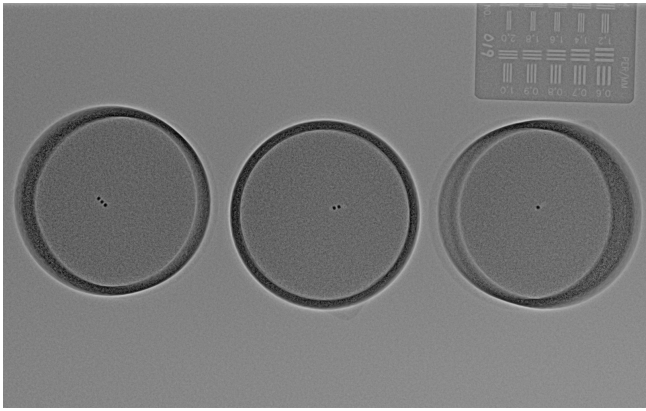
Fig. 8: X-ray of all magnet configurations of the asymmetric helical body in contrast fluid.

B. Stokeslet analysis

In Figure 9, the results of the Stokeslet analysis are displayed. In both translational speed and torque (along the rotation axis) response graphs, there is a linear relation. Furthermore, the analysis displayed that the axial torques at all frequencies remain low and stable over time, indicating that the design's body is stable around the other axes, which is confirmed in the experimental research of Lu *et al.* [8]. Moreover, the change of rotational direction did not have any influence on the absolute translational speeds and torques. The Stokeslet estimation will be used to substantiate the experimentally determined frequency response of the asymmetric helical body, which is discussed in the next subsection.

C. Frequency response

To assess the frequency response, the UMRs were moved back and forth by changing the rotational direction of the RPM. The x-position was then obtained using the camera footage and the Tracker software, and peaks were selected using the script of Appendix C. The peak selection results are displayed in Appendix E. To assess the speed on a run, the linear part between peaks was selected and the average speed was calculated over this part. This was done for at least three runs. From all the average speeds of a single orientation, a mean average speed and standard deviation were calculated and plotted. The orientation of the UMR was manually selected using the video footage.

The first experiment was performed by actuating the symmetrical helical UMR that was used in the experiment that is depicted in Figure 4a. To validate the setup, the frequency response in water between setups is compared in Figure 10.

In the linear part of the frequency response, the results show a good resemblance with a slight y-axis translation of 1.5 mm/s. Around the step-out frequency, which lies around 15-16 Hz, the results start to differ more, which can be caused by the way data is processed or by a slight difference between setups. For example, the RPM position could differ slightly, which would influence the magnitude of the local magnetic field (Formula 2) at the UMR and therefore reduce torque, since $\tau = \mathbf{m} \times \mathbf{B}$. It is noticeable that the step-out frequency is almost equal (15Hz and 16Hz, factor 0.9375) for both measurements, but the translational speed at this frequency is not. Now we know how the data of the setup relates to the blood-water comparison setup, we can use this to translate translational speeds in water to translational speeds in blood for this setup. The factor between step-out frequencies of the setups is 0.9375 and between blood and water in the setup of Figure 4a 1.52, which is 0.66 if translated from water to blood (derived in section II-B). If these factors are multiplied, the factor between the step-out frequency of water in this setup and the step-out frequency in blood is 0.62.

Next, the asymmetric helical body is analysed. The frequency response of this design is illustrated in Figure 11. The first noticeable result is that there is a significant difference between translational speeds with different orientations of the UMR which does not match the theoretical data as shown in section III-B. Moreover, the configuration that has the highest translational speed at any given actuation frequency is the UMR with 2 magnets. Then, the 1-magnet configuration follows. The UMR with the lowest speeds is the 3-magnet configuration. The configuration which resembles the Stokeslet estimation best is the UMR with 1 magnet.

The reason why the actuation frequency is increased up to 40 Hz and not higher is because this is the frequency where the motor of the RPM cannot spin any faster. This was first noticed by a non-changing sound of the motor after 42 Hz. After that, it was double-checked by filming the motor with Nyquist frequency.

The step-out frequency of the UMRs can be roughly estimated by their frequency response. Namely, this is the frequency where the translational velocity starts to decline. In Figure 11a, this point lies around 35 Hz at which the translational speed lies around 35 mm/s. However, for the other UMRs, the translational velocity does not seem to decline. This is an important result since this means that the step-out frequency and therefore maximum translational speed cannot be determined in this experimental setup.

In all frequency responses, there is a linear increase in forward speed visible. For the 1-magnet configuration, this is up until the step-out frequency. For the 3-magnet configuration, this does not directly seem like the case, but when looking into the data (Appendix 15), it seems that for the 25 and 35 Hz measurements, there is an insufficient number of runs per orientation, which results in a higher translational speed. The backward speed, on the other hand, seems, in the case of the 1- and 2-magnet configurations, to reach an equilibrium.

To estimate step-out frequency and translational speed in blood, the relation between the frequency responses in water of the current setup and the water-blood comparison setup and the relation between the water and blood frequency responses of the blood-water comparison setup is used. Firstly, the step-out frequency in blood is determined using the factor (0.62) between step-out in water in the current setup and
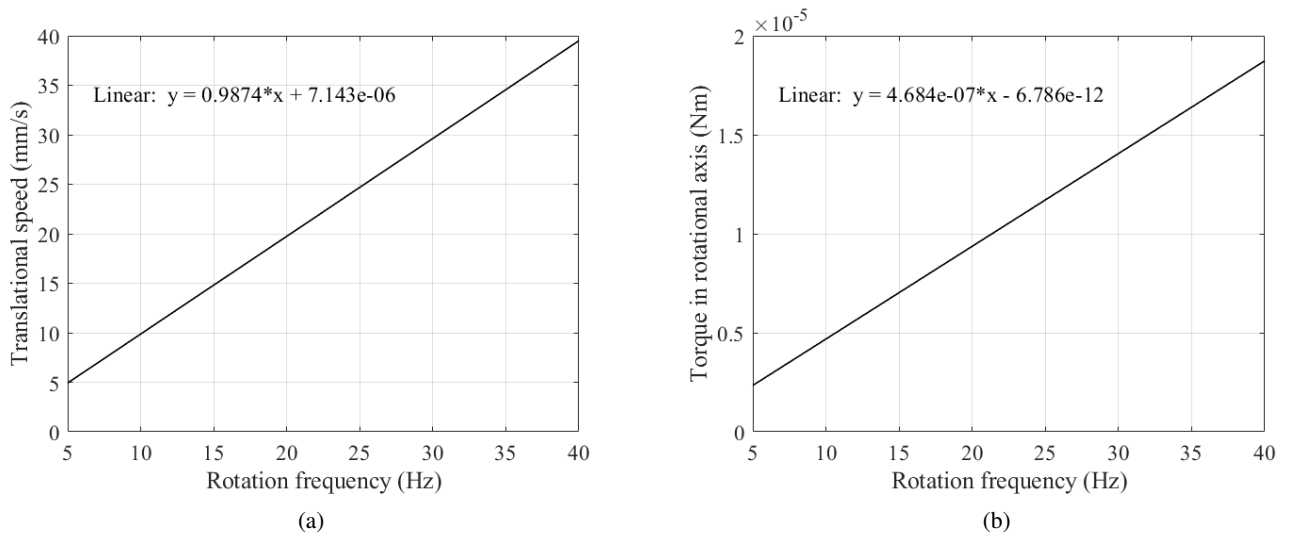
Fig. 9: From the Stokeslet analysis, we derive a theoretical frequency response in water. Here, (a) translational speed and (b) torque in the rotational axis at varying frequencies are illustrated.
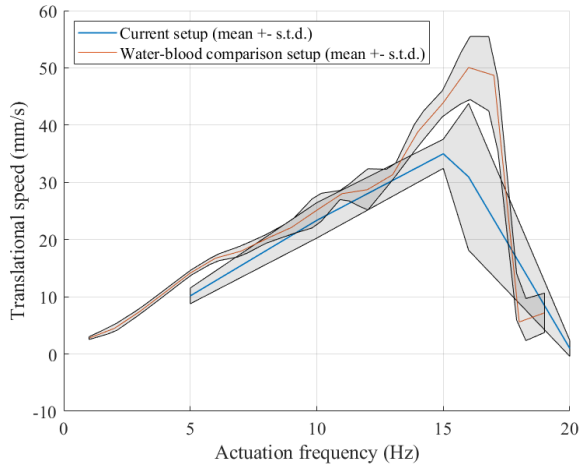

Fig. 10: Frequency response of the symmetrical helical UMR in water in the current setup and the setup that was used to characterize the influence of increased viscosity on the translational speed of the UMR.

step-out in blood in the water-blood comparison setup that was determined from the setup validation measurements. For the 1-magnet configuration, this would mean a step-out frequency of 21.7Hz. Because below step-out frequency in blood a good relation between translational speeds can be derived (see Figure 4a), the slope up until this frequency can be calculated using a linear fit, which can then be translated using the relation between slopes in water and blood (factor 1.14, blood to water) that is determined in section II-B. The slope of the 1-magnet configuration frequency response in water up until its estimated step-out in blood is 1.07 ($R^2 = 0.9952$). Using this, the slope of the frequency response in blood is then estimated to be 0.94. Assuming that the speed goes to zero when the actuation frequency goes

to zero, this results in an estimated maximum translational speed in no-flow blood of 20,40 mm/s for the asymmetric helical body with one magnet.

For the other two magnet configurations, the step-out frequency in water could not be experimentally determined. However, suppose we assume that the linear drag torque remains equal for all magnet configurations since the UMR geometry and environment are equal. In that case, the step-out frequency in blood of the other magnet configurations can be computed from the estimated step-out of the first UMR in blood. Using the theory of section II-B and Formula 3, this would mean step-out frequencies of 46.2 Hz and 69.3 Hz and, using the slope of the measurements (1.502 and 1.173 for 2- and 3-magnet configuration respectively) translated to blood, maximum translational speeds of 60.87 mm/s and 71.31 mm/s are estimated for the 2- and 3-magnet configurations respectively. However, as stated before, the RPM is limited at 42Hz, which is why the advantages of adding more magnets cannot be fully exploited.

D. Flow response

To assess the flow response, the UMRs were moved back and forth by changing the rotational direction of the RPM. However, at higher flow rates, the UMRs were not able to turn fast enough so flow could be overcome. Furthermore, when changing the direction of the UMR using the rotational direction of the UMR, the device seemed to flip inconsistently. Testing this, it seemed that the UMR would rarely flip when positioned directly underneath the RPM and when it was further away it would flip randomly. To reduce measurement time and increase the length of runs, and because of this improve the success rate of measurements, it was decided to hold the UMR with a permanent magnet and release it for every run. For the runs that were done before this change in approach, a similar analysis strategy as the frequency response was used. However, for the other runs
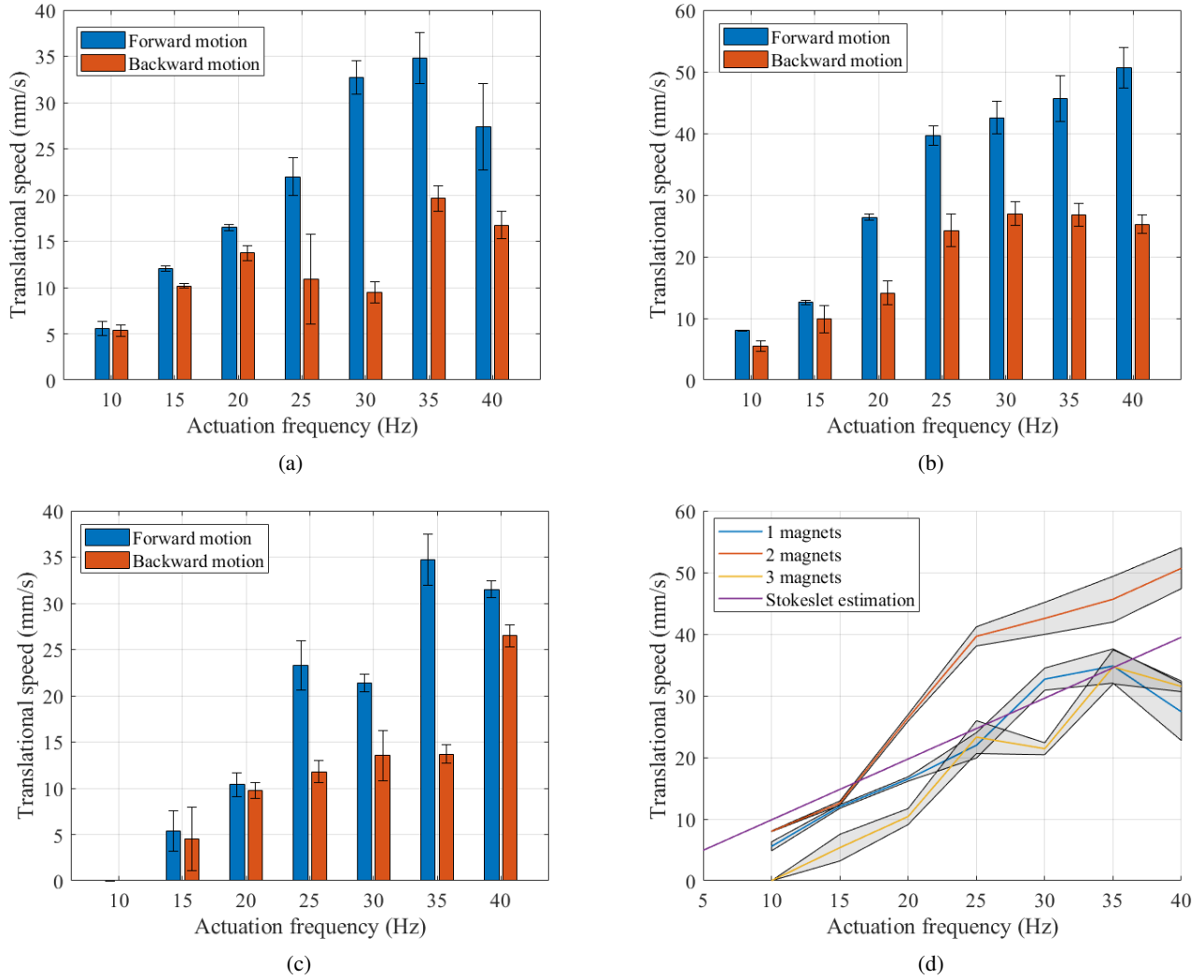
Fig. 11: (a-c) From the frequency response experiment, the frequency response of each magnet configuration, from 1 to 3 respectively, was obtained. Here, forward motion indicates motion where the cone-shaped head of the asymmetric helical body points towards the swimming direction and backward motion where the head points opposite the swimming direction. (d) These forward responses were then plotted against each other including the previously discussed Stokeslet estimation.

a new approach had to be used. Now, there are no peaks, but pieces of x-position data. The start and the end of every piece of data were selected and the average speed within this piece was calculated using a linear fit. Orientation was again selected manually. The scripts of the flow response can be seen in Appendix D and the resulting peak selection in Appendix F.

Firstly, the flow response of the symmetrical helical design in water and blood is compared in Figure 12. Here, an equal actuation frequency (9Hz) and the step-out frequencies of the UMRs in water (9Hz) and blood (14Hz) are used. For each of the measurements, a clear relation with the flow is visible. Comparing the measurements with flow and against flow at an actuation frequency of 9Hz, higher translational speeds are visible for the blood measurement with flow and the water measurements against. This can be explained by the higher viscosity of blood. It causes a

stronger influence of the fluid on the UMR. This influence does not seem to vary with increased flow. Maximum flow rate is derived first. Assuming that the linear trend of the flow response continues for higher flow rates the estimated maximum flow the symmetrical helical UMR can withstand is determined by calculating the intersection with the x-axis. For the 9Hz in blood measurement, this is 72.70 ml/min ($R^2 = 0.9793$), for 9Hz in water this is 82.47 ml/min ($R^2 = 0.9986$) and for 14Hz in water, this is 124.47 ml/min ($R^2 = 0.9421$). The slope of the measurements is equal for both of the 9Hz measurements and slightly steeper for the 14Hz measurements (-0.1338 and -0.1414). Therefore, for the same frequency, one can assume a translation of the y-axis and consequently maximum flow by a factor of 1.134, which is comparable to the slope increase of the frequency response from blood to water without flow, which is 1.14 as determined in section II-B. The slight difference might be
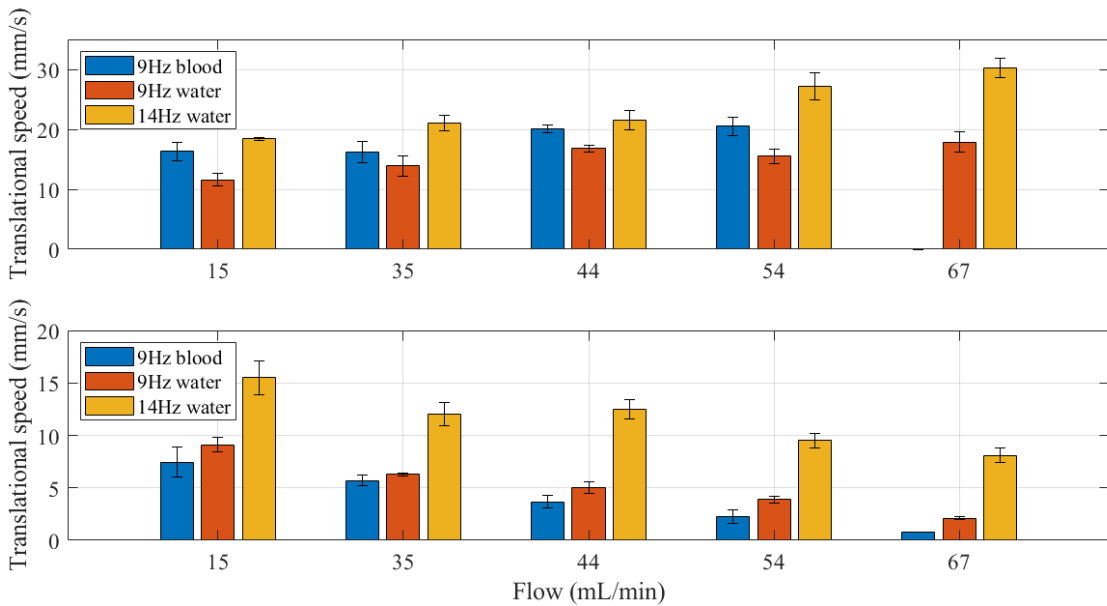
Fig. 12: Flow responses of the symmetrical helical design with varying actuation frequency in blood (of the *ex-vivo* experiment) and water. The first graph shows measurements with flow and the second graph shows measurements against flow.

caused by the difference between this *in-vitro* setup and the *ex-vivo* setup (e.g. cylinder-to-vessel ratio). It is difficult to say what causes the steeper slope of the 14Hz measurement. The linear drag torque coefficient at low Reynolds should stay the same for both measurements. At higher Reynolds, the drag coefficient decreases which would cause the slope to decrease, which is not the case. Because of this, it is assumed that the variance of the measurements themselves causes the steeper slope. The lower R^2 and the slight difference of the linear fit of the 14Hz measurement supports this claim. However, due to the difference in slope, the factor of the y-axis translation cannot be determined with certainty. For this, extra tests should be performed.

Secondly, after the relation between flow in water and flow in the *ex-vivo* setup with blood of the symmetrical helical design is experimentally determined using the previous measurements (Figure 4b), the asymmetric helical body configurations are tested likewise. Like the frequency response, there is a difference between speeds at different orientations visible in Figure 13. However, the backward motion does not seem to reach an equilibrium but instead has a directly proportional relation to the forward motion at increased flow rates. Furthermore, for the 3-magnet measurements, there were no measurements of movement with flow at forward motion below a flow of 67. This is because, with the old approach of changing direction by changing the rotation direction of the RPM, this movement would simply not occur. Since this information is not of great relevance to the outcome of the experiment, it was decided to leave these measurements out.

Lastly, comparing magnet configurations in Figure 14, one can observe that the flow response of forward motion against

the flow and backward motion with the flow is similar for all magnet configurations. However, for the measurements of forward motion with flow, the 3-magnet configuration performs significantly worse than the other two configurations. For backwards motion against flow, the 3-magnet configuration performs best followed by the 2-magnet and 1-magnet configurations respectively. To determine the maximum flow the UMR can withstand with forward motion against the flow, these measurements are extrapolated in the same way that was done for the symmetrical helical design. From this, a maximum flow in water of 283.54 ml/min ($R^2 = 0.9716$), 252.79 ml/min ($R^2 =$) and 286.70 ml/min ($R^2 = 0.9619$) for 1 to 3 magnets respectively was derived. Using the factor of flow response in water to the flow response in blood in the ex-vivo setup, maximum flows of 250.03 ml/min, 222.92 ml/min and 252.82 ml/min for 1 to 3 magnets respectively in the ex-vivo setup are estimated.

V. DISCUSSION

In this chapter, the key findings of the research are discussed. Based on the outcomes of this discussion, recommendations will be Formulated.

A. Key findings

Firstly, this research showed that the swimming performance of the UMR was different for each orientation. This is visible in Figure 11 and 13. This was not visible in the results of the Stokeslet analysis as depicted in III-B. It is most likely that this is because of a difference in translational friction due to a difference in geometry. The cone shape of the head has by definition a lower friction constant than a circular flat surface. Therefore, the backward motion experiences more drag force and therefore
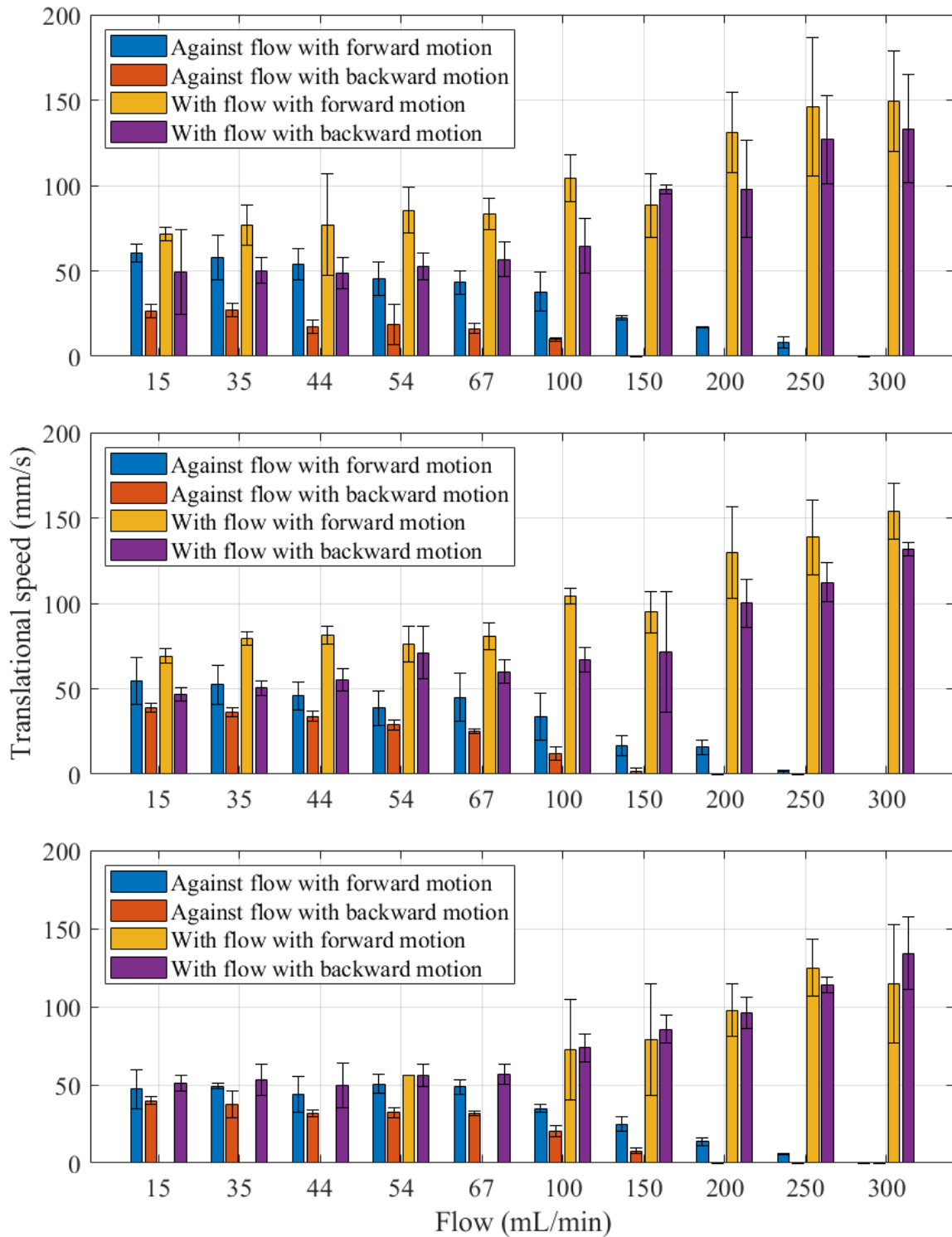
Fig. 13: Flow responses of the asymmetric helical body with 1, 2 and 3 magnets in water respectively.

has lower translational speeds according to Formula 6 and 9.

Secondly, in both the frequency and flow response there was a linear relation with increased frequency and flow respectively. Underneath step-out, the actuation frequency matches the rotational speed of the UMR. The Stokeslet analysis result in Figure 9 showed a linear relationship between this rotational speed and translational speed. As for the flow response, the drag force is linearly dependent on speed with low Reynold numbers, this linear increase in drag force due to flow results in a linear decrease in speed if swimming against flow and a linear increase when
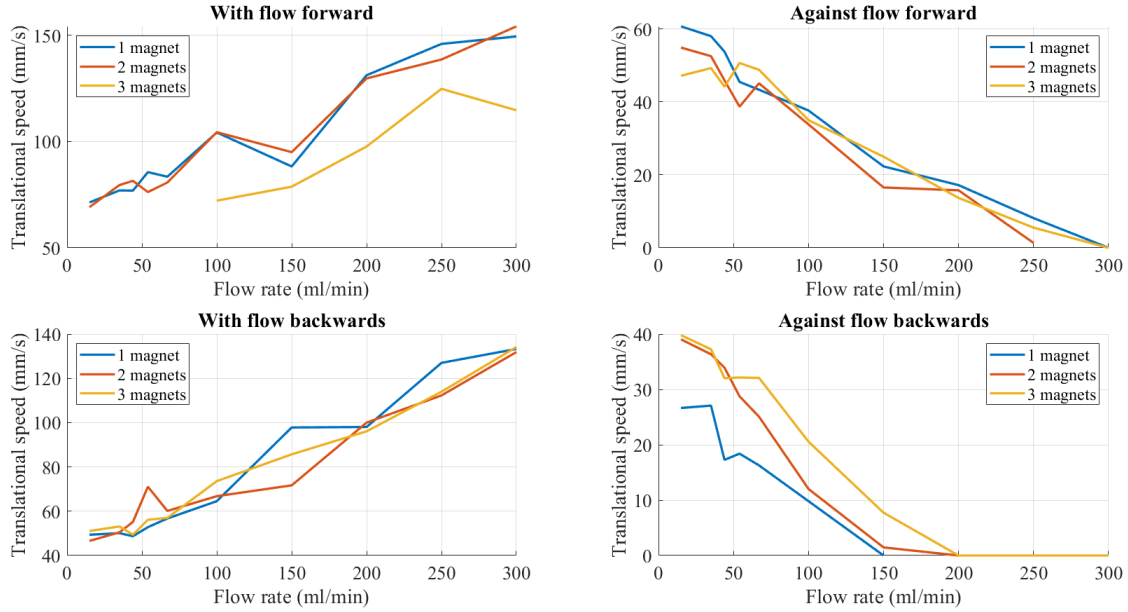
Fig. 14: In this figure, the flow responses of the magnet configurations are compared per orientation and swimming direction.

swimming with flow.

Thirdly, there is a differing frequency response below the step-out frequency for each magnet configuration of the asymmetric helical body. As can be seen in Figure 11d, the UMR with 2 magnets performs much better than the 3 magnet UMR. According to Formula 1 and 3, the torque should linearly increase with higher magnet volume. When the rotational drag coefficient remains equal for each magnet configuration, this would result in a higher step-out frequency and therefore higher translational speeds.

The first possible explanation for the difference between magnet configurations is the increase in mass of the UMR. When looking at the force balance (Formula 9), the increase in mass leads to a higher gravitational force component. Assuming no influence of F_μ and F_m in the y-axis, this would mean that F_n will compensate for the increase in mass. As described in section II-A, this will lead to an increase in (translational and rotational) friction. This in return results in lower translational speeds according to the force balance equation. Since these friction forces are not dependent on speed as seen in the friction force Formula in II, this should result in a negative y-axis translation in the frequency response for higher magnet volume.

This, however, is not the case for the 1-magnet to 2-magnet frequency response, since an increase in translational speed is visible. Therefore, there must be additional forces in play here. Since for this experiment, the RPM position and actuation frequency are kept constant, Formula 3 is not satisfied which results in a magnetic force that attracts the UMR to the RPM. From the video footage, it can be seen that the 1-magnet configuration is greatly influenced by the magnetic force. A couple of observations can be

made: Firstly, the UMR is alternating towards and away from the RPM at lower frequencies, secondly, the UMR barely touches the lower lumen wall and thirdly, when swimming away from the magnet, the magnet seems to follow an upwards path which could be caused by the magnetic field of the RPM. The first observation can be explained by Formula 5, which implicates that magnet attractive force varies for the angle of the RPM. The second and third observations could indicate that the magnetic force is coupled for the complete range of motion of the UMR, which would mean that the magnetic force also has a significant influence on forces on the x-axis, resulting in lower speeds when further away from the magnet. For the other two magnet configurations, this behaviour was not observed. This could indicate that the magnetic force can no longer overcome the gravitational and viscous force generated by the heavier UMRs. Therefore, the difference in frequency response between magnet-configuration can be explained by the influence of magnetic coupling for smaller magnet volume and frictional force for heavier UMRs. This is an interesting result since this could indicate that translational speeds for the 1-magnet UMR can be increased by disabling the magnetic coupling, which can be done by increasing the RPM distance to the tube. This would create friction with the lumen, which could decrease the step-out frequency according to Formula 3, but since the frictional force is linear to the weight of the UMR, it is expected to result in even higher translational speeds than the 2 magnet configuration.

Looking at the results of magnet configuration comparison in flow as depicted in Figure 14, the difference in the behaviour of the UMRs seems to be less evident. Reviewing video footage of the 1-magnet UMR, the influence of magnetic force seems to be less evident as well. Since

this is also the case for the no-flow measurement that was taken before initiating flow, this is most likely to be caused by a difference between setups. The introduction of flow can further explain the equal behaviour of the magnet configurations. For low Reynolds numbers, flow is laminar [16]. The flow within a tube has a parabolic flow velocity profile according to Poiseuille's law. Gou *et al.* [17] describe that Poisseuille flow induces two inertial lift forces: a shear-gradient-induced lift force and a wall-induced lift force. Due to the parabolic velocity profile, the shear-gradient-induced lift is directed towards the wall. The wall-induced lift force opposes this force. Zhang *et al.* [18] describe that the wall-induced lift is dominant when particles travel close to the wall, which is the case for the UMRs. This vertical force opposes the gravitational force which is why the normal force and therefore friction force is reduced, which could explain the little differences between magnet configurations in flow. If one assumes that this wall-induced lift in flow also lowers rotational drag, according to Formula 3, the step-out frequency in flow is increased compared to the no-flow situation.

Fourthly, it is important to note that the estimations of frequency and flow response of the asymmetric helical body are based on experimental data and several assumptions. For example, with the translation of step-out frequency in water to blood, it is assumed that the ratio between the rotational drag coefficient of the symmetrical helical design in water and blood is equal to the ratio between the rotational drag coefficient of the asymmetric helical body in water and blood. Because of this, the ratio between the step-out frequency of water and blood would be equal for all UMR designs according to Formula 3. However, according to Formula 6, the drag force is dependent on the speed of the UMR relative to the fluid. Since we do not have any experimental data on the response in blood of the asymmetrical helical body, it is difficult to say if the influence of water and blood on the speed of the asymmetrical helical body is the same as this influence for the symmetrical helical design. This speed difference could theoretically be determined by the Stokeslet script since viscosity is one of its inputs. However, the viscosity did not have any influence on the results of the script. Because an influence is expected, the viability of the Stokeslet script needs to be looked into.

Furthermore, it is assumed that the ratio between slopes of water and blood frequency responses below step-out is equal for both UMRs. Whether this assumption is true, depends on the behaviour of the asymmetric helical body in blood as well. The same method of translating slopes based on the ratio of the symmetrical helical UMR is used for the translation of maximum flow from water to blood. Because the experimental results do not consist of many data points, variations have a big influence on the slope. Because these slopes are used for the estimation, this has a direct influence on the accuracy of these estimations. To validate this accuracy, tests in blood with the asymmetric helical body or changes to the Stokeslet script, which allow varying viscosity are necessary.

Moreover, to estimate the step-out in water of the 2- and 3-magnet configurations, it was assumed that the rotational drag coefficient remained equal. However, as discussed for the third key finding, the friction with the lumen is most likely to influence this coefficient. Therefore, in reality, the step-out frequency of the 2- and 3-magnet configuration would be lower than the estimated frequency of 46.2 Hz and 69.3 Hz in blood respectively.

Fifthly, the RPM of the setup has a maximum rotational frequency of 42 Hz. Since the translational velocity is linear with actuation frequencies below the step-out frequency, the translational speed at this frequency is the maximum translational speed of the UMR. Since the step-out in water is not reached for both the 2- and 3-magnet configurations, the maximum velocity in blood could not have been determined experimentally even if the relation between speed in water and blood was known. Because of this, the values were estimated. These estimated values were then translated to the estimated step-out frequency in blood and these values are still above the maximum actuation frequency of the motor. This indicates that withstanding the highest possible blood flow would currently be limited by the RPM for higher magnet volume. Therefore, the advantage of having more magnets cannot be exploited using the current setup.

Lastly, there is inconsistent control of the asymmetric helical body using an RPM. In the frequency response experiment, it became apparent that the UMR tends to flip randomly if the swimming direction is changed when it is not directly under the RPM. When the direction is changed underneath the RPM this flipping happens less often but it was not consistent. This might be due to the asymmetrical design or the imbalance caused by the position of the magnets within the UMR as seen in Figure 8. In a clinical environment, this would present difficulties. When the UMR is inside a lumen for which X-ray imaging is necessary, the orientation of the UMR is difficult to identify due to the lack of absorbance by the UMR body as seen in Figure 8. Because the tip of the UMR must be pointed towards the thrombus to allow the most efficient drilling, identification of orientation is necessary. A possible solution for when 3 magnets are used, is magnet spacing. Before insertion, the clinician would make an X-ray of the assembled UMRs and select one where a clear difference between spacing between magnets is visible. By identifying at which end the tip is, the clinician knows the orientation inside the lumen when an X-ray is used. However, for less magnets, this cannot be used. Another solution would be to create a symmetrical body or to find a way of actuating the UMR without flipping inconsistently.

B. Recommendations

First of all, it is necessary to perform frequency and flow experiments in blood for the asymmetric helical body to see

if the translation of frequency and flow responses from water to blood can be directly translated to other UMR designs and to validate the accuracy of the estimations made in this research. By doing this, future experiments with other UMR designs can be assessed in water which diminishes logistical problems e.g. the supply of blood and the increased difficulty of imaging the UMR in blood.

Second of all, to overcome the high flow rate of the aorta, the maximum actuation frequency of the RPM should be increased. This is currently the limiting factor. Since the advantage of having more magnets cannot be exploited because of this factor, it is recommended to use the lightest UMR to reduce friction with the lumen.

Last of all, to counter random flipping of the UMR when changing swimming direction, a change in the control method or a design change towards a symmetrical design needs to be considered.

VI. CONCLUSIONS

The goal of this study is to assess the swimming performance of the asymmetric helical body with a varying amount of magnets in the X-ray-guided robotic platform and to assess the feasibility of this design for feature research.

From this research, an effective method for the assembly of the asymmetric helical body UMRs was derived, the viability of using X-ray imaging to visualise the position and orientation of the UMR was validated, frequency and flow response experiments were successfully performed with both the old symmetrical helical design and the asymmetric helical body with different magnet configurations and the performance of these UMRs in blood was estimated using the experimental data gathered in this research and previous experiments of the research group.

From the research several key findings became evident. Firstly, the UMRs showed different translational speeds for each orientation, where backward motion was slower in nearly every case. Secondly, the frequency and flow response both showed a linear relation with increased frequency and flow respectively. Thirdly, in the frequency response results, the different magnet configurations showed a different frequency response below the step-out frequency. Fourthly, the step-out frequencies of the asymmetric helical body in blood in no-flow are estimated to be 21.7 Hz, 46.2 Hz, and 69.3 Hz for 1 to 3 magnets respectively. Moreover, the maximum flow the asymmetric helical body can withstand in blood (in *ex-vivo*) at 40 Hz, is estimated to be 250.03 ml/min, 222.92 ml/min and 252.82 ml/min for 1 to 3 magnets respectively. However, it should be noted that these estimations are based on experimental data and several assumptions which is why these might prove to be inaccurate. Fifthly, it became apparent that the RPM has a maximum rotational frequency of 42 Hz which was reasoned to be the limiting factor for achieving higher translational speeds. Lastly, the asymmetric helical body shows random orientation flipping behaviour when the swimming direction is changed.

Following these results, recommendations are made to ensure further development towards the application of UMRs in clinical practice and in further research. First of all, to validate the viability of directly translating the performance of different UMR designs in water to blood to greatly improve the feasibility of *in-vitro* experiments, frequency and flow responses of the asymmetric helical body have to be tested in blood as well. Second of all, to overcome the high flow rate of the aorta, the maximum actuation frequency of the RPM should be increased. Last of all, to counter random flipping of the UMR when changing swimming direction, a change in the control method, where the RPM is no longer stationary, or a design change towards a symmetrical design needs to be considered.

REFERENCES

[1] N. S. Key and R. S. Kasthuri, "Current Treatment of Venous Thromboembolism," *Arteriosclerosis, Thrombosis, and Vascular Biology*, vol. 30, no. 3, pp. 372–375, 3 2010. [Online]. Available: https://www.ahajournals.org/doi/10.1161/ATVBAHA.109.197145

[2] C. Kearon, S. R. Kahn, G. Agnelli, S. Goldhaber, G. E. Raskob, and A. J. Comerota, "Antithrombotic Therapy for Venous Thromboembolic Disease," *Chest*, vol. 133, no. 6, pp. 454S–545S, 6 2008. [Online]. Available: https://linkinghub.elsevier.com/retrieve/pii/S0012369208601245

[3] Y. R. Manda and K. M. Baradhi, *Cardiac Catheterization Risks and Complications*, 2024. [Online]. Available: http://www.ncbi.nlm.nih.gov/pubmed/26673558http://www.pubmedcentral.nih.gov/articlerender.fcgi?artid=PMC4777042

[4] B. MU and B. J, "Thrombolytic Therapy," 2023. [Online]. Available: https://www.ncbi.nlm.nih.gov/books/NBK557411/

[5] H. Shen, S. Cai, Z. Wang, Z. Ge, and W. Yang, "Magnetically driven microrobots: Recent progress and future development," *Materials & Design*, vol. 227, p. 111735, 3 2023. [Online]. Available: https://linkinghub.elsevier.com/retrieve/pii/S0264127523001508

[6] J. Leclerc, Y. L. Lu, A. T. Becker, M. Ghosn, and D. J. Shah, "Resonating Magnetic Manipulation for 3D Path-Following and Blood Clot Removal Using a Rotating Swimmer," in *2020 IEEE/RSJ International Conference on Intelligent Robots and Systems (IROS)*. IEEE, 10 2020, pp. 3083–3090. [Online]. Available: https://ieeexplore.ieee.org/document/9340746/

[7] J. Leclerc, H. Zhao, D. Bao, and A. T. Becker, "In Vitro Design Investigation of a Rotating Helical Magnetic Swimmer for Combined 3-D Navigation and Blood Clot Removal," *IEEE Transactions on Robotics*, vol. 36, no. 3, pp. 975–982, 6 2020. [Online]. Available: https://ieeexplore.ieee.org/document/9098916/

[8] Y. Lu, J. Ramos, M. G. Ghosn, D. J. Shah, A. T. Becker, and J. Leclerc, "Insertion, Retrieval and Performance Study of Miniature Magnetic Rotating Swimmers for the Treatment of Thrombi," in *2023 IEEE/RSJ International Conference on Intelligent Robots and Systems (IROS)*. IEEE, 10 2023, pp. 8454–8460. [Online]. Available: https://ieeexplore.ieee.org/document/10342355/

[9] L.-J. W. Ligtenberg, N. C. A. Rabou, S. Peters, T. Vengetela, V. Schut, H. R. Liefers, M. Warlé, and I. S. M. Khalil, "Remote Control of Untethered Magnetic Robots within a Lumen using X-Ray-Guided Robotic Platform," in *IEEE International Conference on Robotics and Automation (ICRA)*, Yokohama, 2024. [Online]. Available: https://www.researchgate.net/publication/378109088_Remote_Control_of_Untethered_Magnetic_Robots_within_a_Lumen_using_X-Ray-Guided_Robotic_Platform

[10] I. Khalil, R. Lomme, V. Magdanz, A. Klingner, E. Klein, R. Lipocoat, B. V. Colin, H. E. Nijland, L. B. V. Dorothee, W. Lipocoat, B. V. Pascal, J. Lipocoat, H. Liefers, A. Susarrey-Arce, and M. Warle, "Ex Vivo Validation of Magnetically Actuated Intravascular Untethered Robots in a Clinical Setting," *Under review*, 2023. [Online]. Available: https://doi.org/10.21203/rs.3.rs-3526473/v1

[11] A. W. Mahoney and J. J. Abbott, "Managing magnetic force applied to a magnetic device by a rotating dipole field," *Applied Physics Letters*, vol. 99, no. 13, 9 2011. [Online]. Available: https://pubs.aip.org/apl/article/99/13/134103/340960/Managing-magnetic-force-applied-to-a-magnetic

[12] T. W. R. Fountain, P. V. Kailat, and J. J. Abbott, "Wireless control of magnetic helical microrobots using a rotating-permanent-magnet manipulator," in *2010 IEEE International Conference on Robotics and Automation*. IEEE, 5 2010, pp. 576–581. [Online]. Available: http://ieeexplore.ieee.org/document/5509245/

[13] Huaming Li, Jindong Tan, and Mingjun Zhang, "Dynamics modeling and analysis of a swimming microrobot for controlled drug delivery," in *Proceedings 2006 IEEE International Conference on Robotics and Automation, 2006. ICRA 2006*. IEEE, pp. 1768–1773. [Online]. Available: http://ieeexplore.ieee.org/document/1641962/

[14] K. Avila, D. Moxey, A. de Lozar, M. Avila, D. Barkley, and B. Hof, "The Onset of Turbulence in Pipe Flow," *Science*, vol. 333, no. 6039, pp. 192–196, 7 2011. [Online]. Available: https://www.science.org/doi/10.1126/science.1203223

[15] J. R. Rumble, *CRC Handbook of Chemistry and Physics*, 99th ed. Boca Raton: CRC Press, 2018.

[16] B. Rehm, D. Consultant, A. Haghshenas, A. S. Paknejad, and J. Schubert, "Situational Problems in MPD," in *Managed Pressure Drilling*. Elsevier, 2008, pp. 39–80. [Online]. Available: https://linkinghub.elsevier.com/retrieve/pii/B9781933762241500085

[17] Y. Gou, Y. Jia, P. Wang, and C. Sun, "Progress of Inertial Microfluidics in Principle and Application," *Sensors*, vol. 18, no. 6, p. 1762, 6 2018. [Online]. Available: http://www.mdpi.com/1424-8220/18/6/1762

[18] J. Zhang, S. Yan, D. Yuan, G. Alici, N.-T. Nguyen, M. Ebrahimi Warkiani, and W. Li, "Fundamentals and applications of inertial microfluidics: a review," *Lab on a Chip*, vol. 16, no. 1, pp. 10–34, 2016. [Online]. Available: http://xlink.rsc.org/?DOI=C5LC01159K

A. Stokeslet script

See *BSc Assignment\Stokeslet*. Written by A. Klinger.

B. RPM actuation script

See *BSc Assignment\RPM_RoboDK_Matlab\RPM_RoboDK_Matlab* file *RPMMan.m*. Written by L.W. Ligtenberg.

C. Frequency response analysis script

See *BSc Assignment\Lab experiment 2 - frequency response\Tracker* files *main.m* and *SpeedAnalysis.m.*

D. Flow response analysis script

See *BSc Assignment\ Lab experiment 1 - response in flow\ Tracker* files *main.m*, *FlowAnalysis.m*, *FlowAnalysisHouston.m* and *barplotter.m*.
The main file selects which *FlowAnalysis* script to use according to a manually given input and uses the results from this script to plot the data. However, for measurements where both the regular *FlowAnalysis* and *FlowAnalysisHouston* are used, the *barplotter* is used to merge the results and plot these.

E. Linear track selection results of the frequency response scripts
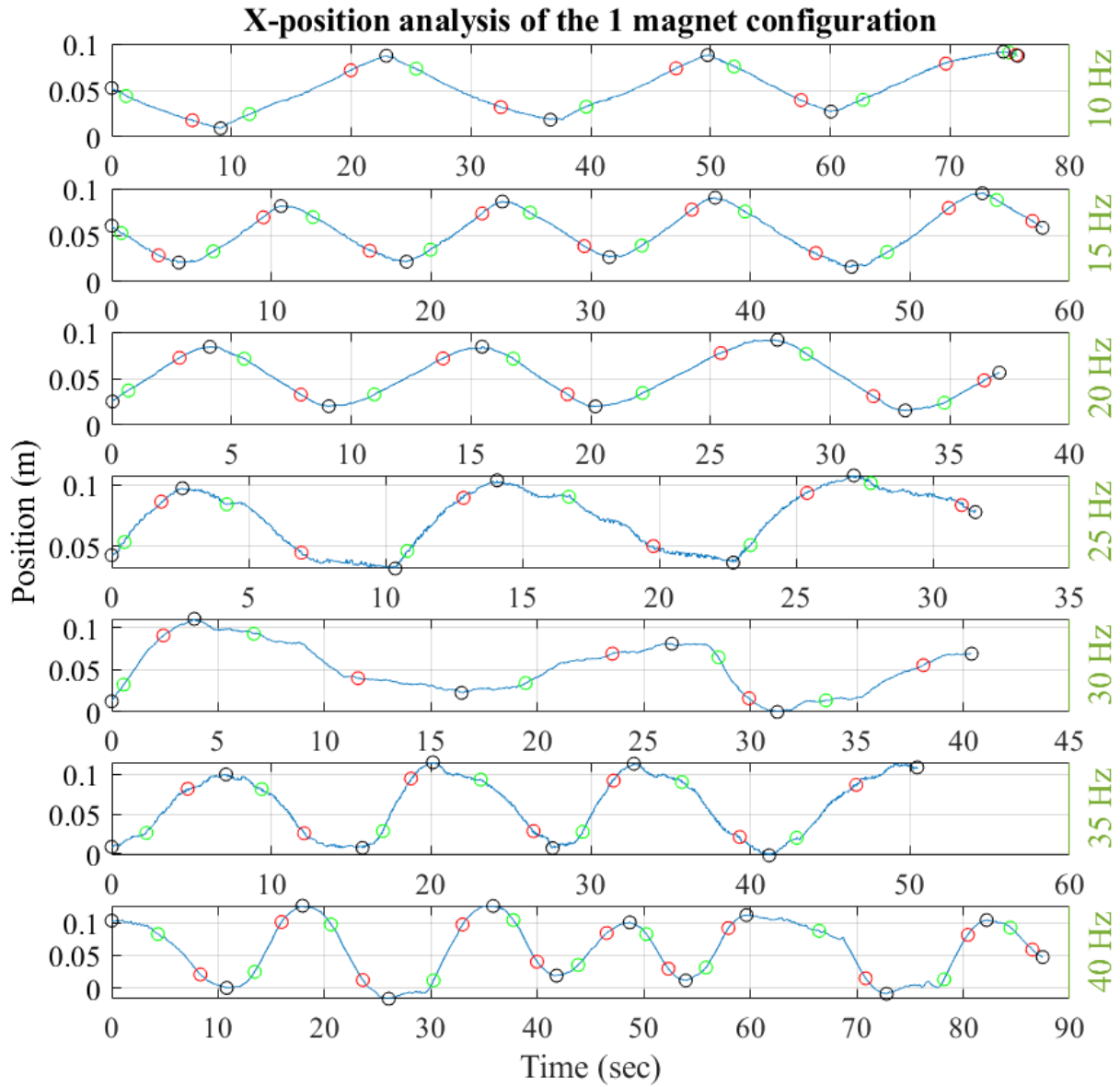
Fig. 15: X-position analysis results of the scripts from Appendix C of the 1 magnet configuration.
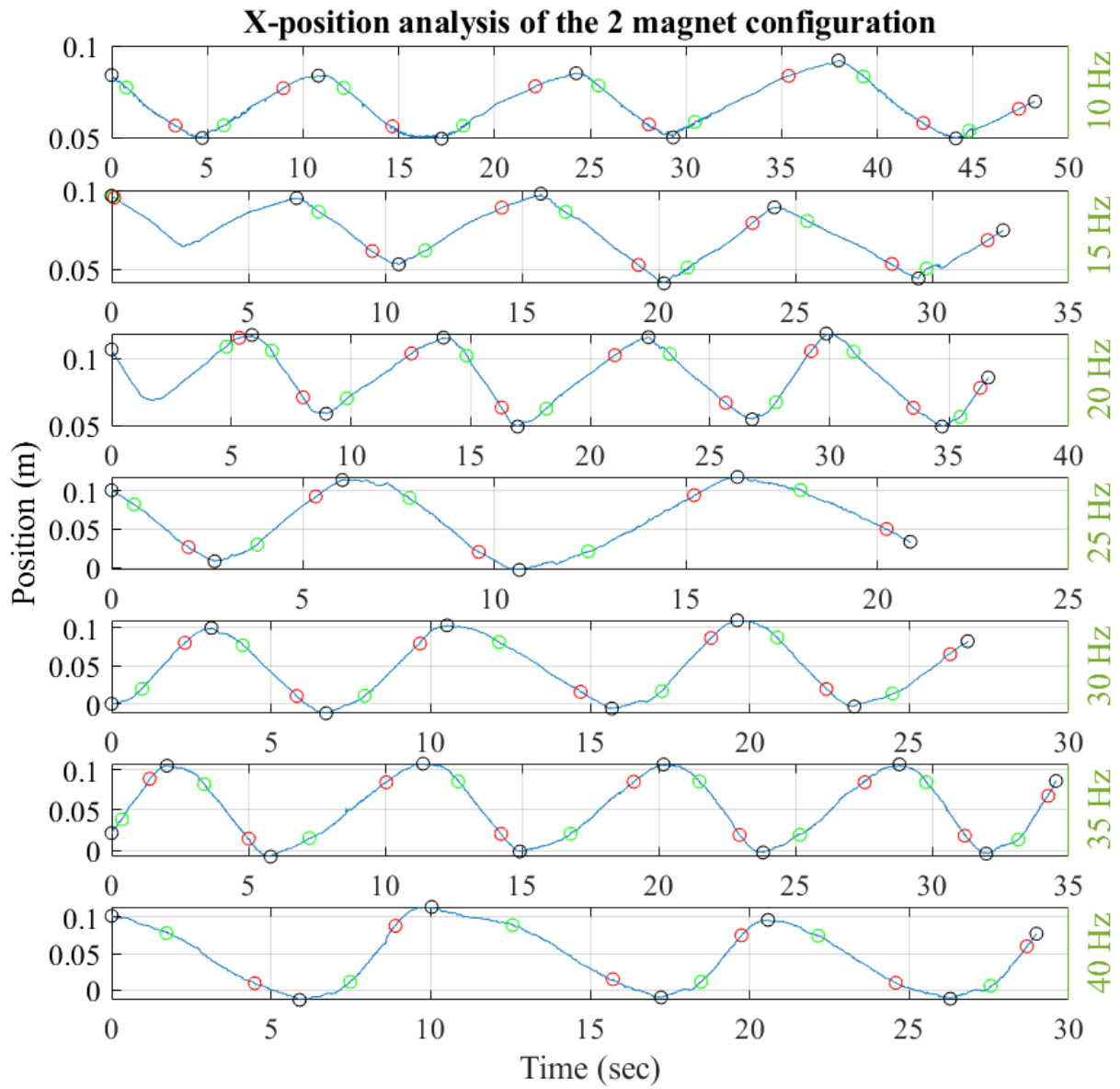
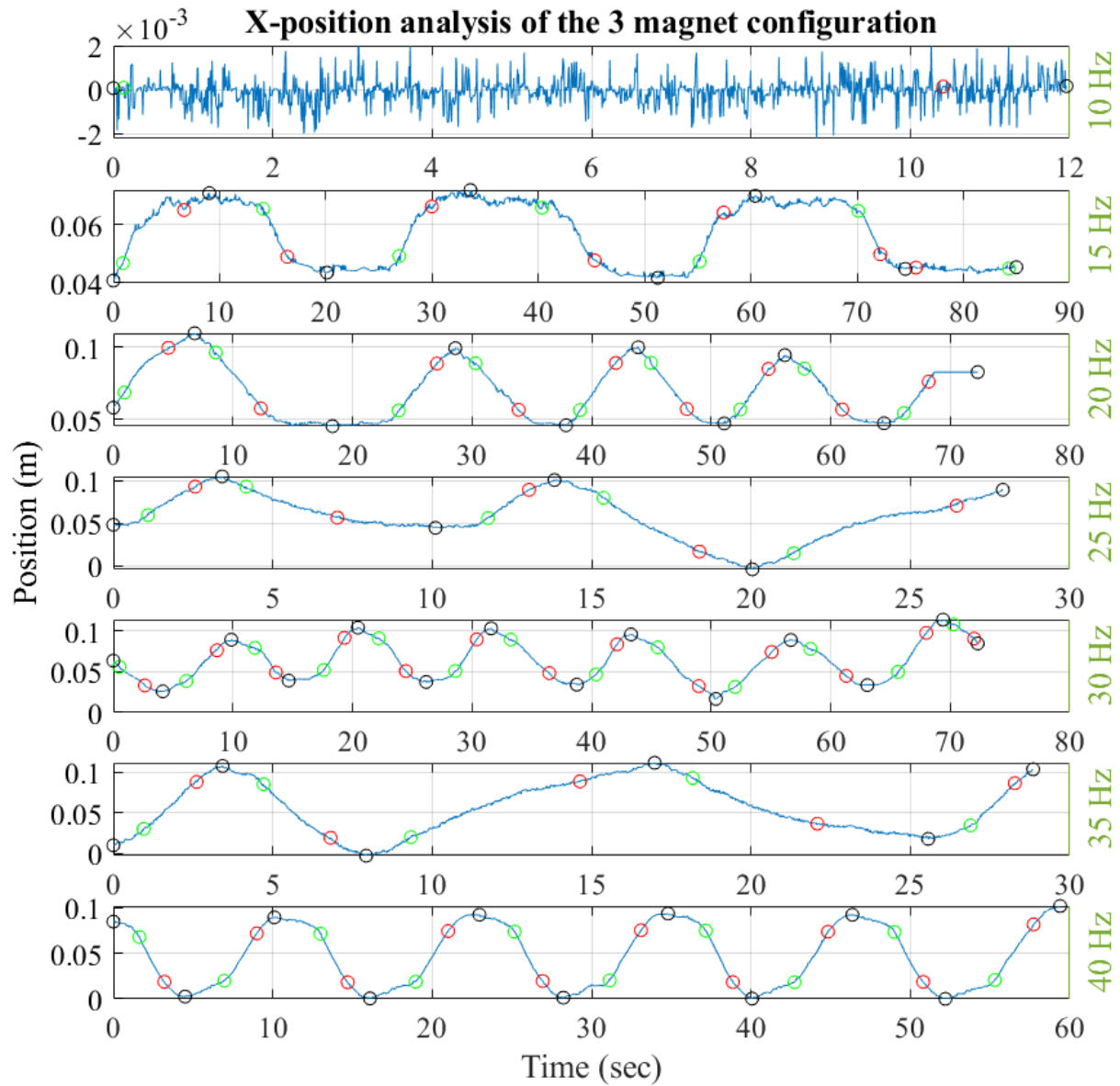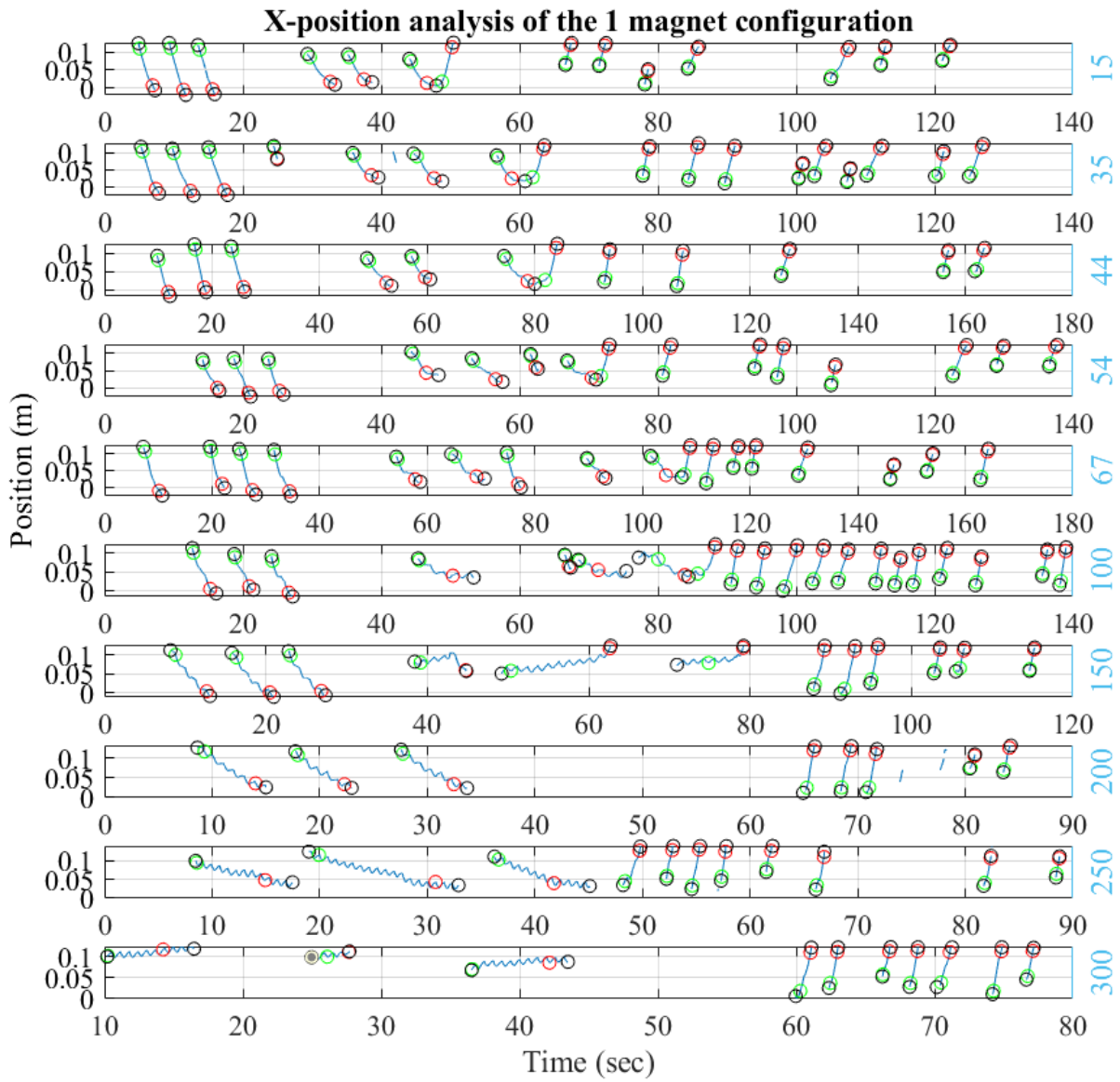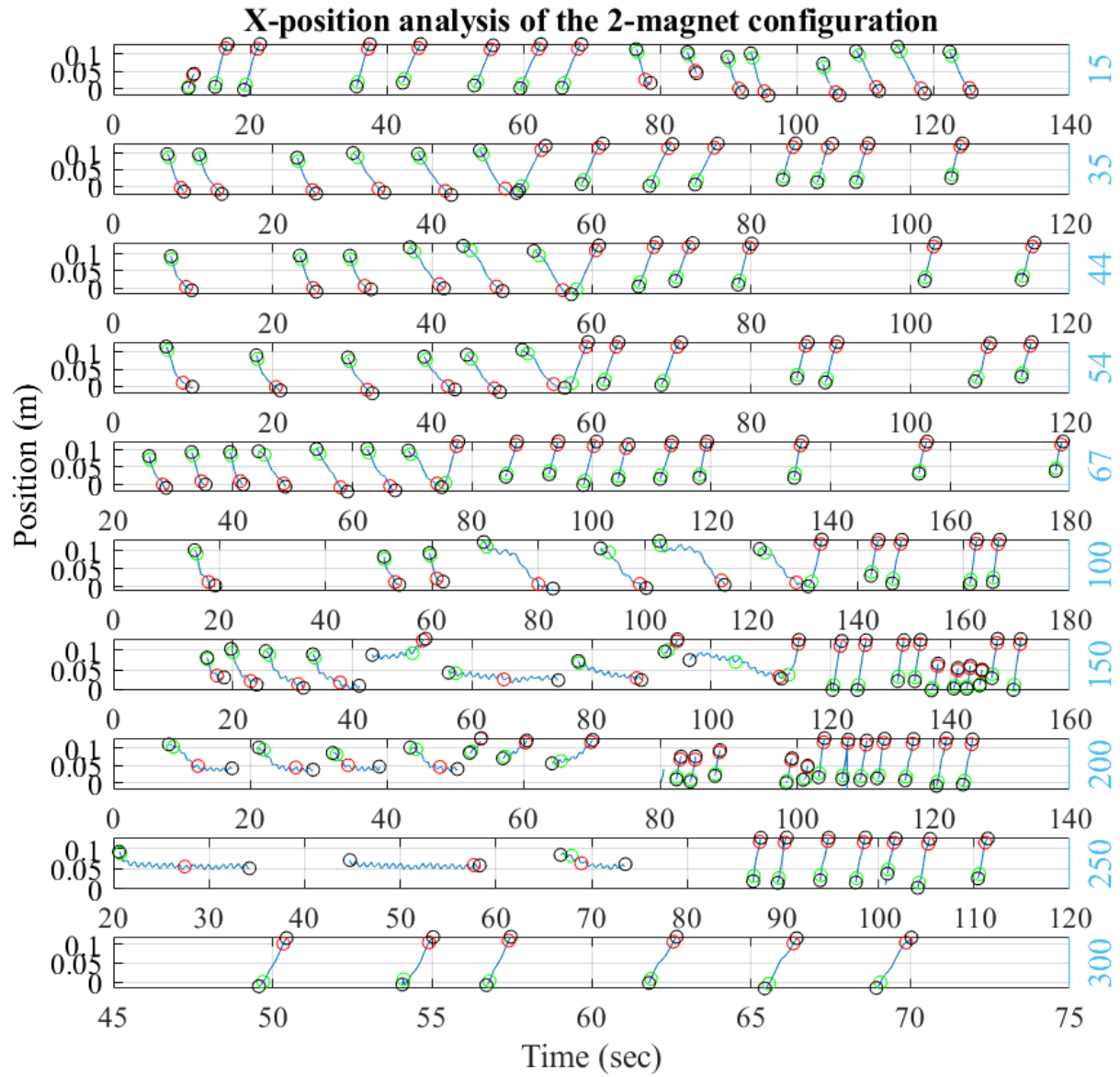Fig. 16: X-position analysis results of the scripts from Appendix C of the 2 magnet configuration.

Fig. 17: X-position analysis results of the scripts from Appendix C of the 3 magnet configuration.

Fig. 18: X-position analysis results of the scripts from Appendix D of the 1 magnet configuration.

Fig. 19: X-position analysis results of the scripts from D of the 2 magnet configuration.
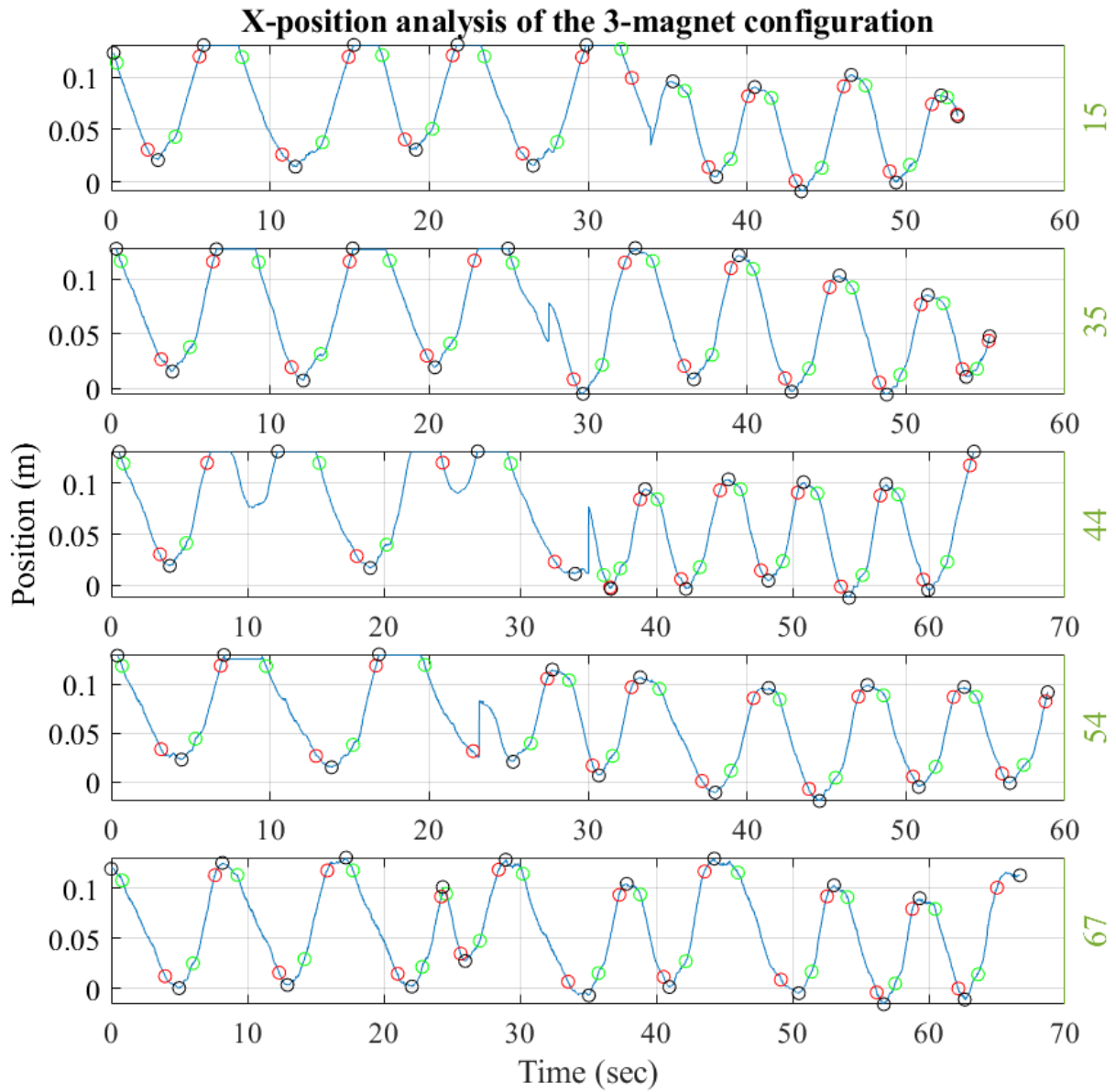
Fig. 20: X-position analysis results of the scripts from Appendix D of the 3 magnet configuration below 67 ml/min.
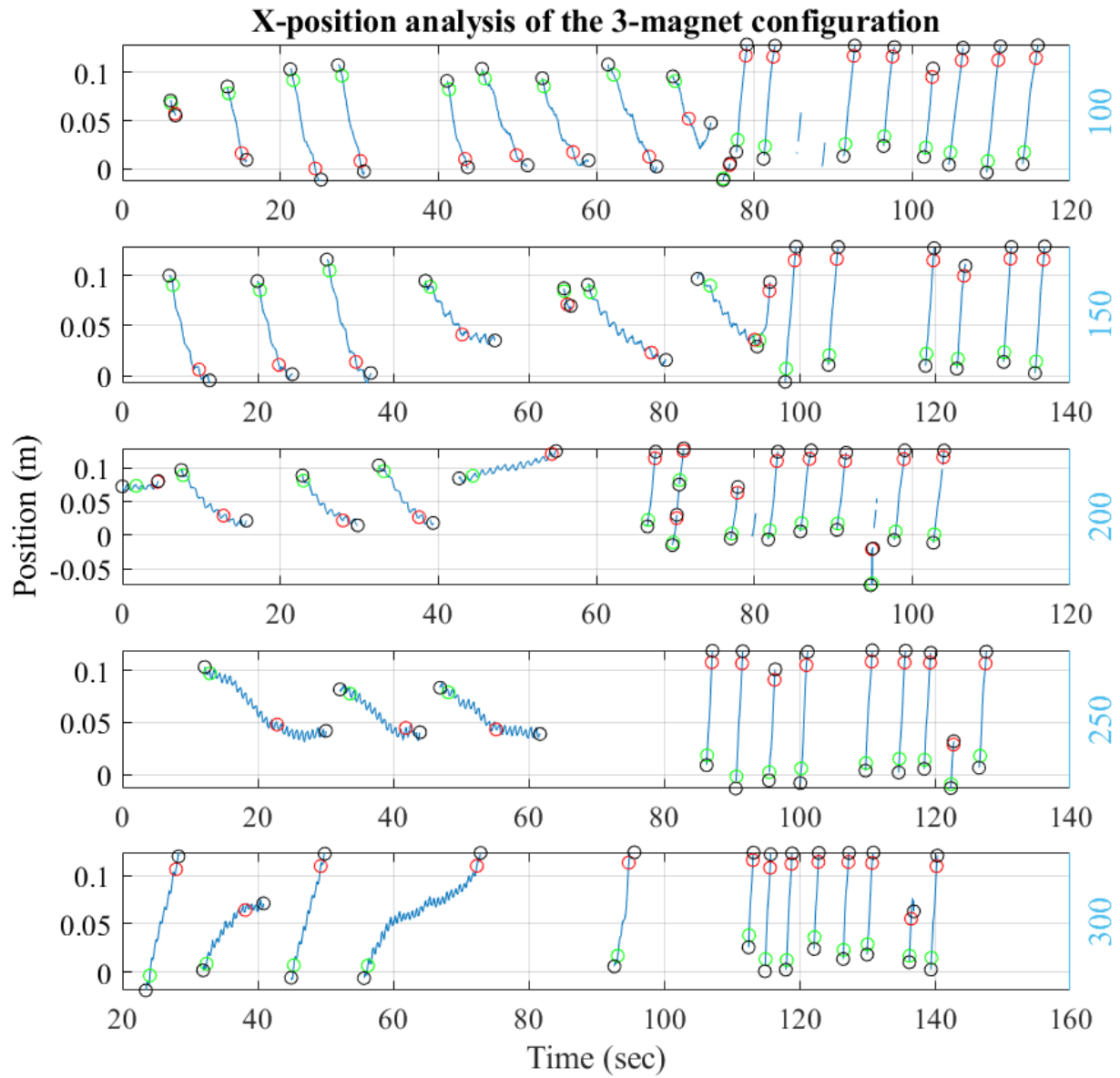
Fig. 21: X-position analysis results of the scripts from Appendix D of the 3 magnet configuration Above 67 ml/min.